REPORT DOCUMENTATION PAGE

Form Approved
OMB No. 0704-0188

1. REPORT DATE (DD-MM-YYYY)	2. REPORT TYPE	3. DATES COVERED (From - To)
26-06-2007	FINAL REPORT	July 2004 - March 2007

4. TITLE AND SUBTITLE
Development of highly ordered, heterostructured semiconductor nanowire arrays for optical devices

5a. CONTRACT NUMBER
FA9550-04-1-0435

5b. GRANT NUMBER

5c. PROGRAM ELEMENT NUMBER

6. AUTHOR(S)
Harry Ruda
Selvakumar Nair

5d. PROJECT NUMBER

5e. TASK NUMBER

5f. WORK UNIT NUMBER

7. PERFORMING ORGANIZATION NAME(S) AND ADDRESS(ES)
University of Toronto
Department of Materials Science and Enginering
184 college St
Toronto M5S3E4, Canada

8. PERFORMING ORGANIZATION REPORT NUMBER

9. SPONSORING / MONITORING AGENCY NAME(S) AND ADDRESS(ES)
US Air Force Office of Scientific Research
875 N Randolph St
Arlington VA 22203

10. SPONSOR/MONITOR'S ACRONYM(S)

11. SPONSOR/MONITOR'S REPORT NUMBER(S)

12. DISTRIBUTION / AVAILABILITY STATEMENT
Distribution Statement A: unlimited

AFRL-SR-AR-TR-07-0472

13. SUPPLEMENTARY NOTES

14. ABSTRACT
Methodology for efficient growth of semiconductor nanowires of several II-VI (ZnSe, ZnO, ZnS) and III-VI (GaAs, InSb) nanowires was developed and optimized. Based on optical and transport characterization measurements, defect states responsible for quenching of band-edge luminescence were identified and post-growth treatments were devised to eliminate those defects and to achieve strong excitonic emission. Carrier trapping dynamics was elucidated by ultrafast time-resolved optical pump-probe measurements. Optimized ZnSe nanowires were shown to exhibit an exceptionally high photoconductive response of 22A/W in a single nanowire transistor device. Manganese doped ZnO nanowires were fabricated and above room temperature ferromagnetism was achieved. Transport measurements showed these wires to be n-type with a degenerate carrier distribution. The experimental efforts were supplemented by modeling that included design of high Q-factor nanowire array photonic cavities using as well as a theory of excitons in nanowires.

15. SUBJECT TERMS
Semiconductor nanowire, VLS growth, photodetector, magnetic semiconductor, exciton, photonic crystal

16. SECURITY CLASSIFICATION OF:			17. LIMITATION OF ABSTRACT	18. NUMBER OF PAGES	19a. NAME OF RESPONSIBLE PERSON
a. REPORT	b. ABSTRACT	c. THIS PAGE		30	19b. TELEPHONE NUMBER (include area code)

FINAL REPORT

July 2004-March 2007

Title of project:	Development of Highly Ordered, Heterostructured Semiconductor Nanowire Arrays for Sub-wavelength Optical Devices
Duration of the project:	July 2004 – March 2007
Funding Number:	AFOSR Grant FA9550-04-1-0435
Principal Investigator:	Prof. Harry Ruda
Personnel involved:	Prof. H. Ruda Dr. Z. Wu Dr. A Shik Dr. S. Nair Dr. U. Philipose Mr T. Xu Mr. J. Salfi
Publications:	List attached
Performing Institution:	University of Toronto
Address:	184 College Street Department of Materials Science and Engineering University of Toronto Toronto ON M5S 3E4 Canada

LIST OF PUBLICATIONS

1. T. Xu, S. Yang, S. V. Nair and H. E. Ruda, "Confined modes in finite-size photonic crystals", Phys. Rev. **B 2**, 045126 (2005).

2. S. Yang, T. Xu, H. E. Ruda and M. Cowan, "Numerical study of anomalous refraction in photonic crystals", Phys. Rev. **B 72**, 075128 (2005).

3. H. E. Ruda, A. Shik, "Polarization sensitive optical phenomena in semiconducting and metallic nanowires", Phys. Rev. B **72**, 115308 (2005).

4. H. E. Ruda, "Properties and applications of photonic crystals" in "Optical properties of condensed matter and applications", Ed. J. Singh, J. Wiley & Sons (2005).

5. T. Xu, S. Yang, S. V. Nair, and H. E. Ruda, "Nanowire array based photonic crystal devices", Proc. SPIE Int. Soc. Opt. Eng. **5971**, 597115 (2005)

6. U. Philipose, H. E. Ruda, A. Shik, C. F. de Souza, and P. Sun, "Light emission from ZnSe nanowires", Proc. SPIE Int. Soc. Opt. Eng. **5971**, 597116 (2005)

7. Z. H. Wu, J. Gierak, E. Bourhis, A.-L. Biance, and H. E. Ruda, "Highly oriented and ordered semiconductor nanowire arrays for photonic device applications" Proc. SPIE Int. Soc. Opt. Eng. **5971,** 597117 (2005)

8. Shik, H. E. Ruda and I .G. Currie, "Electromechanical and electrooptical properties of nanowires" J. Appl. Phys **98**, 094306 (2005)

9. Harry E. Ruda and Alexander Shik, "Polarization-sensitive optical properties of metallic and semiconducting nanowires", Proc. SPIE Int. Soc. Opt. Eng. **6099**, 60990L (2006)

10. M. Ikezawa, S. V. Nair, H.W. Ren, Y. Masumoto and H. E. Ruda, "Biexcitons in parabolic quantum dots", Phys. Rev. B. **73**, 125321 (2006).

11. M. Blumin, H.E. Ruda, I. Savelyev, A Shik and H. Wang, "Self-assembled InAs quantum dots and wires grown on a cleaved-edge GaAs(100) surface", J. Appl. Phys. **99**, 093518 (2006).

12. U. Philipose, H.E. Ruda, A. Shik, C. DeSouza and P. Sun, "Conductivity and photoconductivity in undoped nanowire array", Appl. Phys. Lett. **99**, 066106 (2006).

13. U. Philipose, S. V. Nair, S. Trudel, S, Aouba, R. H. Hill and H. E. Ruda, "High-temperature ferromagnetism in Mn-doped ZnO nanowires", Appl. Phys. Lett., **88**, 263101(2006).

14. H.E. Ruda and N. Matsuura, "Properties and applications of photonic crystals", in series "*Optical properties of condensed matter and applications*", Ed., J. Singh, (J. Wiley & Sons, 2006).

15. K. Koughia, J. Singh, S.O. Kasap and H.E. Ruda, "Fundamental optical properties of materials II", in series "*Optical properties of condensed matter and applications*", Ed., J. Singh, (J. Wiley & Sons, 2006).

16. J. Singh and H.E. Ruda, "Concept of excitons", in series "*Optical properties of condensed matter and applications*", Ed., J. Singh, (J. Wiley & Sons, 2006).

17. H. E. Ruda and A. Shik, "Polarization-sensitive optical phenomena in thick semiconducting nanowires", J. Appl. Phys. **100**, 024314 (2006)

18. U. Philipose, T. Xu, S. Yang, Ping Sun, Harry E. Ruda, Y. Q. Wang, and K. L. Kavanagh, "Enhancement of band edge luminescence in ZnSe nanowires", J. Appl. Phys. **100**, 084316 (2006)

19. J. Salfi, U. Philipose, C. F. de Sousa, S. Aouba, and H. E. Ruda, "Electrical properties of Ohmic contacts to ZnSe nanowires and their application to nanowire-based photodetection", Appl. Phys. Lett. **89**, 261112 (2006)

20. U. Philipose, P. Sun, T. Xu, H. E. Ruda, L. Yang, and K. L. Kavanagh, "Structure and photoluminescence of ZnSe nanostructures fabricated by vapor phase growth", J. Appl. Phys. **101**, 014326 (2007)

21. K. Matsuda, S. V. Nair, H. E. Ruda, Y. Sugimoto, T. Saiki, and K. Yamaguchi, "Two-exciton state in GaSb/GaAs type II quantum dots studied using near-field photoluminescence spectroscopy", Appl. Phys. Lett. **90**, 013101 (2007)

22. J. Salfi, U. Philipose, S. Aouba, S. V. Nair, and H. E. Ruda, "Electron transport in degenerate Mn-doped ZnO nanowires", Appl. Phys. Lett. 90, 032104 (2007)

23. S. V. Nair and H. E. Ruda, "Theiry of excitons in nanowires" (in preparation)

24. H. E. Ruda and A. Shik, "Nonlinear optical phenomena in nanowires", J. Appl. Phys. 101, 034312 (2007)

25. T. Xu, S. Yang, S. V. Nair, and H. E. Ruda, "Nanowire-array-based photonic crystal cavity by finite-difference time-domain calculations", Phys. Rev. B **75**, 125104 (2007)

26. M. Sugisaki, H-W Ren, S. V. Nair, E. Tokunaga, K. Nishi, Y. Masumoto, and H. E. Ruda, "Anisotropic optical response of InP self-assembled quantum dots studied by pump-probe spectroscopy", Phys. Rev. B 75, 125315 (2007)

27. H. E. Ruda and A. Shik, "Polarization and plasmon effects in nanowire arrays", Appl. Phys. Lett. 90, 223106 (2007)

Theses and dissertations

1. Tao Xu, "Modelling of nanowire array based photonic crystal cavity", Masters Thesis submitted to University of Toronto (2005)
2. Usha Philipose, "Growth and characterization of semiconductor nanowires", Ph.D. thesis submitted to University of Toronto (2006)

1 Introduction

Our proposal to develop semiconductor nanowire arrays for sub-wavelength optical applications was funded by AFOSR for the period of July 2004 to March 2007. Prior to this funding we had demonstrated expertise in the growth of high-quality GaAs nanowires by Vapor-Liquid-Solid (VLS) growth using MBE[1]. The key focus of the new work was to (i) achieve high-quality II-VI and III-V nanowires using a more efficient CVD growth approach (ii) suppress deep level emission and reveal excitonic band-edge emission by controlling growth conditions as well as by post-growth treatments (iii) characterize and optimize the nanowire structures by optical and transport measurements and (iv) demonstrate potential for optical device applications. During the 2 years and 9 months of work done under this funding we have made great progress on all of these points. We have also identified several novel features of nanowires, both experimentally and theoretically, that make them very attractive for technological use. The following sections contain a brief description of the main results of our investigations. The work reported here has resulted in one Ph.D. thesis, one Master's thesis and several publications as shown in the list of publications attached. Detailed results including figures, tabulated data, experimental methodology and theoretical formulations may be found in those publications.

2 Growth facility and technique

During the course of this project nanowires of a variety of semiconducting materials including GaAs/AlGaAs, InSb and several II-VI binaries were grown, characterized and optimized. Except for GaAs/AlGaAs nanowires which were grown by MBE, a CVD system was used for all other materials. Leveraging on our previous expertise with

catalyst assisted VLS growth of GaAs nanowires using MBE, an efficient CVD growth approach was developed and optimized for ZnO, ZnS, ZnSe and InSb nanowires. A schematic of the CVD growth setup is shown in Fig. 1.

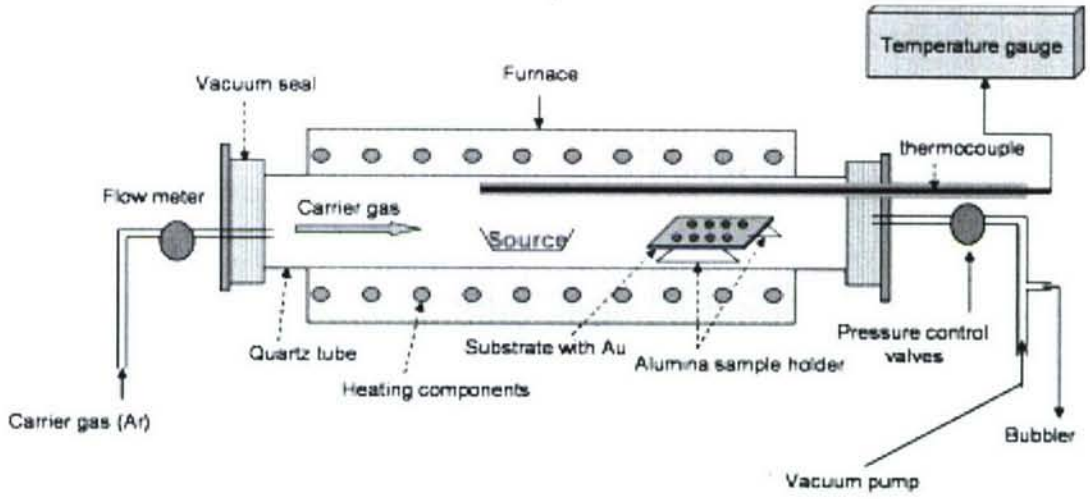

Fig. 1 Schematic illustration of the experimental setup for synthesis of semiconductor nanowires.

The furnace is a single zone resistance heated furnace. It has a specific thermal profile, with a constant temperature zone at the centre of the heating zone and steep temperature gradients at the two ends of the furnace. The maximum working temperature can be set to 1100C. A quartz tube placed inside the tube furnace serves the purpose of the growth chamber. An alumina (Al_2O_3) boat, to contain the source material, and an alumina sample holder, to place the substrate on, are positioned inside the quartz tube during growth. A carrier gas (Argon) is made to flow in through one end of the tube and then the gas and any evolved gases exits through a bubbler, permitting one to perform a reaction under a controlled inert atmosphere. The VLS growth process is illustrated in Fig. 2

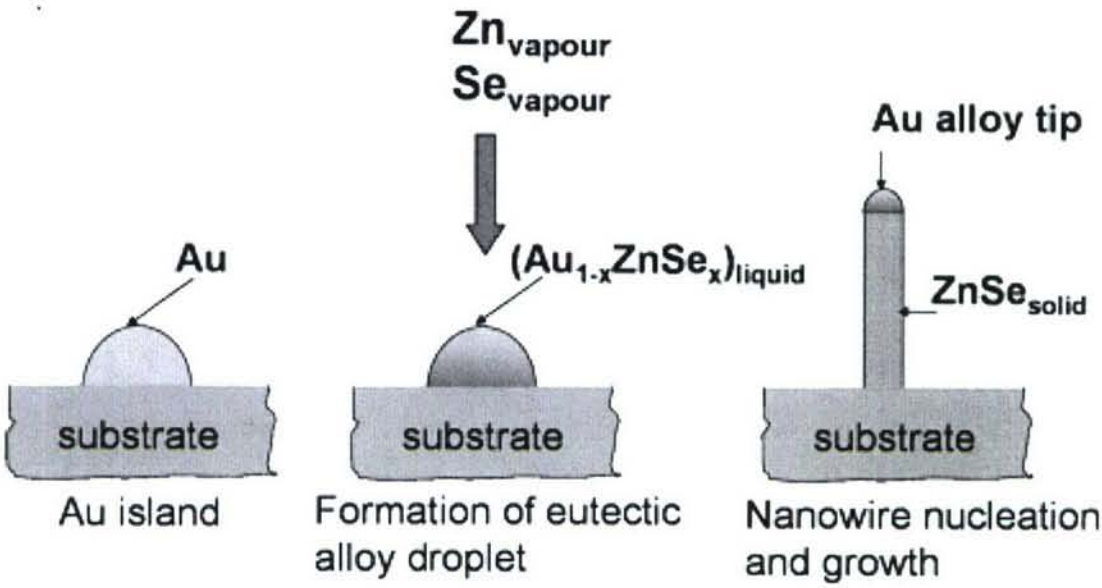

Fig. 2. A schematic showing processes involved in VLS growth.

The growth methodology involves the following steps.

i. Cleaning of the substrate: n-type Si substrates were cleaned by sonicating them in acetone for approximately 30 mins and then etched in 5% HF/H_2O to remove the native oxide and create a hydrogen-terminated surface. Any subsequent rinsing by de-ionized was minimized to retain as much of the H-termination as possible.

ii. Deposition of catalyst film: typically a 50 nm layer of Au film was deposited on the substrate by thermal evaporation.

iii. Loading the furnace: The source material (e.g., pure ZnSe powder) was placed in an alumina boat at the centre of the quartz tube. The Si substrate was placed at one end of the quartz tube, which was then inserted into a horizontal tube furnace, such that the substrate was at the downstream end of the flowing argon (Ar) gas.

Prior to heating, the system was first evacuated to about 120 Torr and then flushed with a high flow of Ar gas (flow rate = 120 sccm) for almost 1 hour to eliminate oxygen

contamination. Under a constant flow of Ar (50 sccm), the furnace was rapidly heated at a rate of 60 C/min to the required source temperature source point and held at this temperature during the growth process, which typically lasted for 1 hour. The substrate temperature which is the growth temperature is generally several 100 degrees lower than the source temperature.

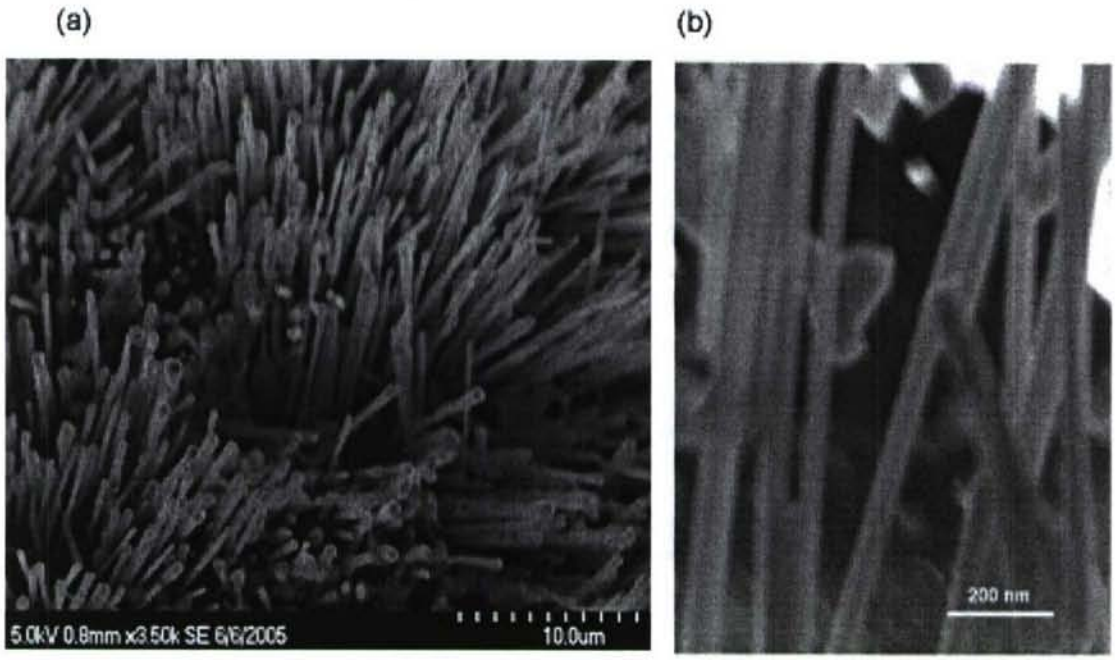

Fig. 3. SEM image of ZnSe nanowires grown on (111) n-Si substrate with thin Au film. The wires had an average length of 8-9 microns and diameters of 40-80 nm.

Fig. 3 shows a typcial SEM image of as grown nanowires. High yield growth of relatively uniform nanowires is apparent from the image. The average length of nanowires shown in Fig. 3 is 8 microns. The length strongly depends on the growth time. For ZnSe a growth rate of 150nm/min was estimated. The diameter of the nanowires is controlled by the size of the gold droplets formed prior to growth which mainly depends on the thickness of the gold film. Finer control over the diameter was achieved using colloidal

gold particles in place of gold film. An example of 20nm diameter ZnSe nanowires grown this way is shown in Fig. 4.

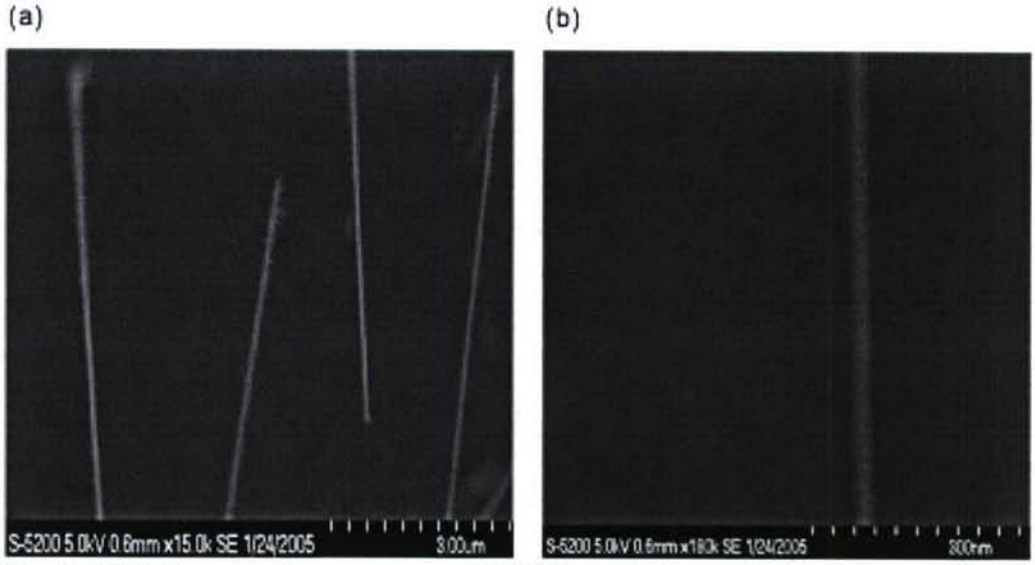

Fig. 4. (a)ZnSe nanowires grown on Si (111) substrates using Au nanoparticles as the seeds for catalytic growth. (b)SEM image of a single ZnSe nanowire on Si substrate. The wire length is about 4 microns and diameter is 20 nm.

High degree of crystallinity of the nanowires was verified by High Resolution TEM (HRTEM) (see Fig 5) and Energy-dispersive X-ray Spectroscopy (EDXS) showed stoichiometric growth of ZnSe nanowires (Fig. 6).

Fig. 5. HRTEM image of ZnSe nanowires revealing its crystalline nature.

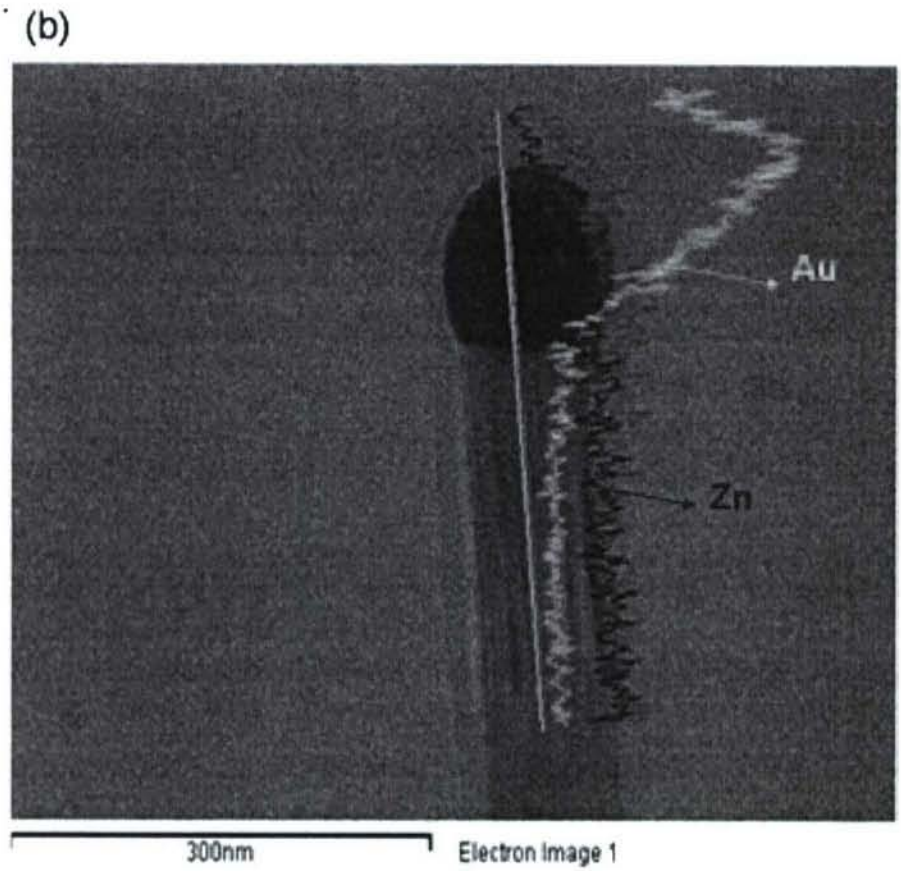

Fig. 6. EDXS spectrum measured for Au-catalysed ZnSe nanowires grown at 650 C. (a) The Zn/Se intensity ratio indicates a stoichiometric ZnSe nanowire. (b) Elemental mapping of the nanowire confirming uniform composition along its length and gold accumulation at the tip.

The growth approach described above is highly versatile and allows for growth of several types of materials with control of the dimensions and composition of the nanowires. Typical SEM images ZnO and ZnS nanowires grown by this method are shown in Figs. 7-8.

The crystalline quality, density of defects and compositional uniformity depends on the growth conditions. A major effort was directed towards optimization of the growth conditions based on feedback from characterization measurements discussed later in this report. For details of optimized growth conditions for various materials see Ref. 2.

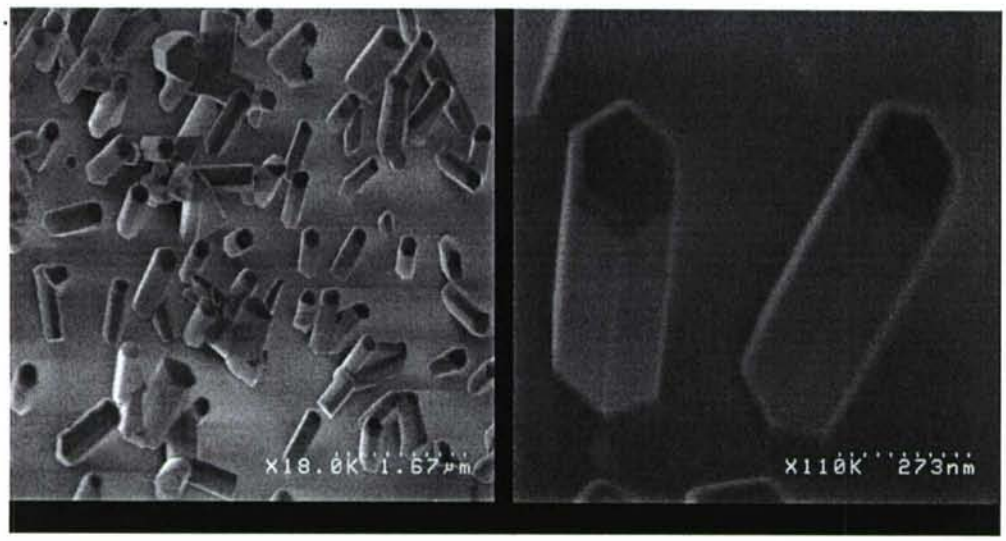

Fig. 7.SEM image of hexagonal ZnO nanowires.

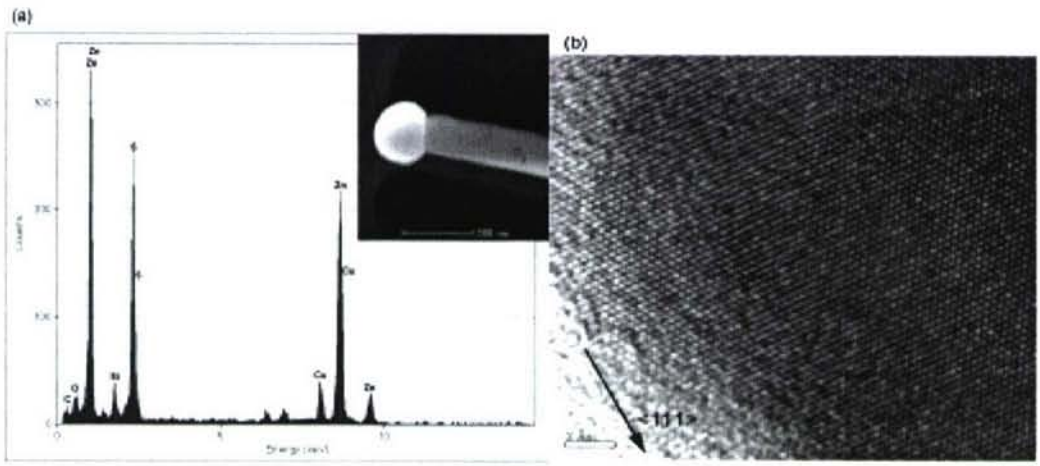

Fig. 8(a). EDXS spectrum confirming the chemical composition of ZnS nanowires. (b) Bright field TEM image of a ZnS nanowire.

2.1 Positional and orientational ordering

While nanowire diameter could be controlled by the size of the gold catalyst droplets as described above, achieving positional and orientational order is more challenging. To this end, we used an alumina template to deposit a periodic array of gold seeds on a GaAs substrate. Subsequent MBE growth of GaAs nanowires by VLS generated well ordered arrays of nanowires with a fixed orientation dependent on the substrate orientation –

vertical on a 111 surface as opposed to 45 degree slanted growth on a 110 surface. Examples of such well ordered growth is shown in Fig. 9. Optical diffraction by the nanowire arrays was used to characterize the ordering and periodicity[3]. Developing this approach further to realize photonic cavities of the type discussed in section 4.1 is of great interest.

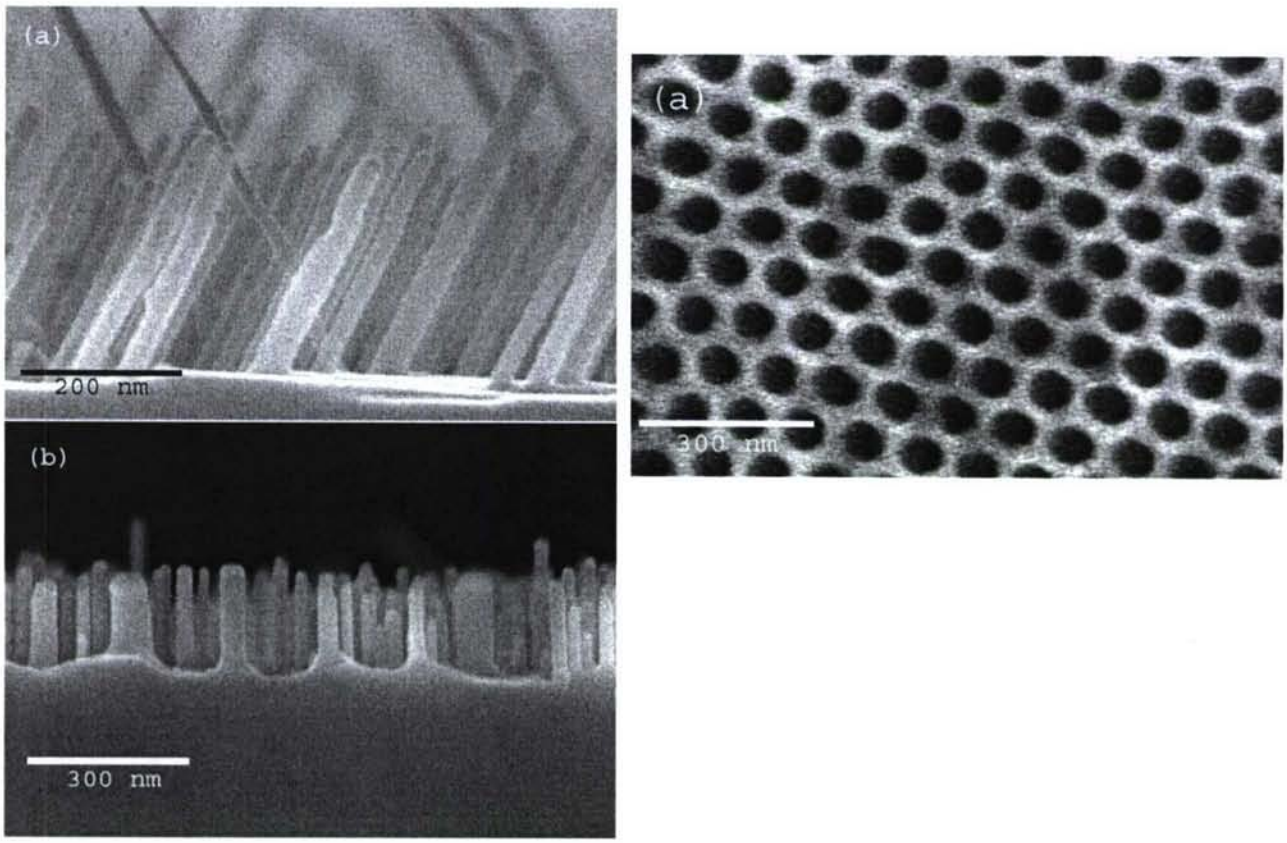

Fig. 9 Inclined and vertical growth of highly ordered and GaAs nanowires on GaAs 110 (top) and 111 (bottom) substrate. Gold catalyst seeds were initially grown through an alumina template (shown on right) to achieve positional ordering.

3 Characterization Experiments and Results

3.1 Photoluminescence and defect state control

One significant problem with II-VI materials has been the difficulty in obtaining stoichiometric nanowires. As a result, such nanowires typically are comprised of high

concentrations of defect complexes that limit their use in optical devices. Considerable effort was directed towrad understanding the factors which affect the crystallinity and stoichiometry how deviations from ideal structure affects the optical properties of nanowires. Through extensive photoluminescence (PL) measurements we have identified growth conditions and post growth treatments under which efficient light emission near the band-edge could be obtained.

A typical room temperature PL spectrum of ZnSe nanowires grown by MOCVD under different growth pressures[4] shows a spectrum dominated by two characteristic emission peaks --- a band edge (BE) emission peak at 2.68 eV (463 nm) and a broad deep defect (DD) related emission peak in the region 1.8-2.4 eV (500 nm to 680 nm). The intensity ratio of BE to DD emission is strongly dependent on the growth conditions. Past efforts at controlling this ratio and especially enhancing the BE emission has met with limited success.

In order to determine the effect of growth conditions on the optical quality of nanowires, three different samples of ZnSe nanowires were synthesized for optical characterization. While HRTEM of near-stoichiometric and Zinc-rich samples showed high degree of crystallinity, a high density of stacking faults and twinning defects was observed in Se-rich samples[5].

Fig. 9 shows the PL spectrum for nanowires grown under near stoichiometric conditions. It is comprised of two emission bands --- a narrow BE peak at 463 nm and a broad DD band extending from ~ 500 nm to 680 nm. The PL spectrum of nanowires grown under Zn-rich conditions is shown in Fig. 10. As can be seen, this spectrum is dominated by BE emission and the emission intensity from the DD states is very weak. Since these nanowires were grown under Zn-rich conditions, the low concentration of Zn vacancies

probably accounts for the very low intensity of the DD emission peak. Conversely, the PL spectrum for nanowires grown under Se-rich conditions (Fig. 11) is dominated by the DD emission, while the amplitude of the BE emission is non-existent. As noted above nanowires grown under high Se vapour flux also contained a high density of structural defects which could be could be responsible for the quenching of BE emission and strong DD emission in these nanowires. A careful study of the dependence of excitation intensity on DD emission[2] shows that this emission peak is due to a donor-acceptor pair (DAP) recombination mechanism involving Zn vacancies as the acceptor species and Zn interstitials or Se vacancies as the donor species.

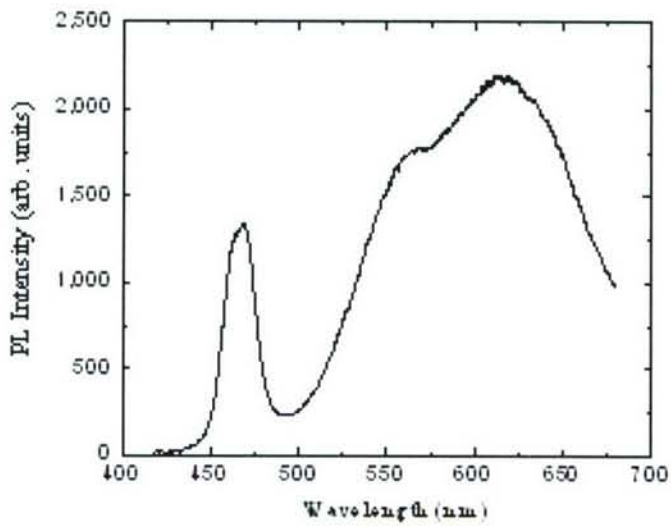

Fig. 9. Room temperature PL spectra of ZnSe nanowires grown under near stoichiometric conditions, showing weak BE emission and strong DD emission.

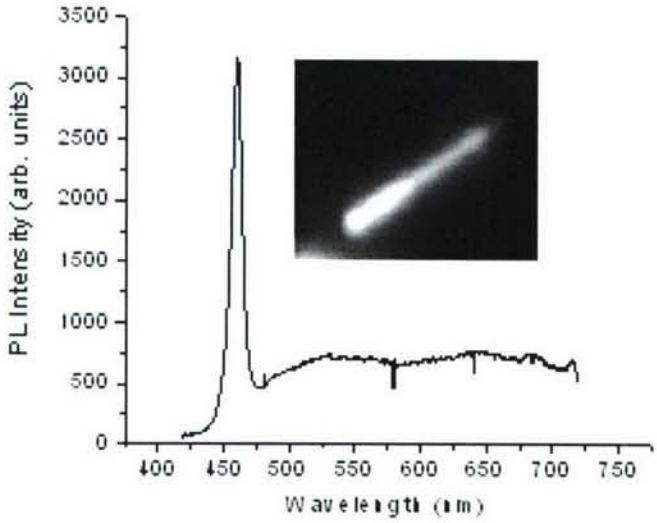

Fig. 10. Room temperature PL spectrum of ZnSe nanowires grown under Zn-rich conditions, showing strong BE emission and very weak DD emission. Inset shows blue luminescence from a single nanowire

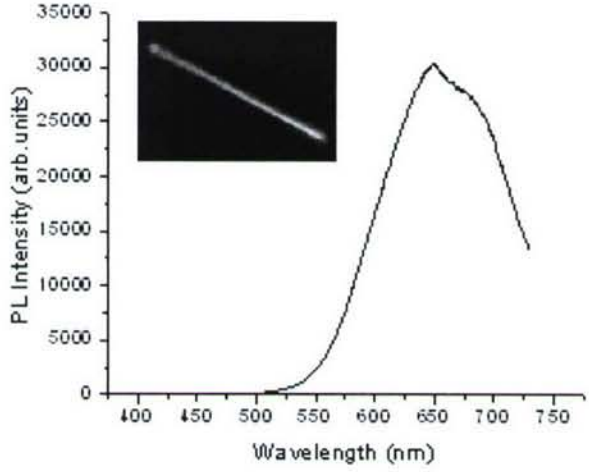

Fig. 11. Room temperature PL spectrum of ZnSe nanowires grown under Se-rich conditions, showing strong DD emission and no emission from the BE states. Inset shows strong red luminescence from a single nanowire

Based on the above results we devised an annealing procedure where as grown nanowires are annealed in a Zn-rich atmosphere that significantly enhances the BE emission as

shown in Fig. 12. The order of magnitude improvement in the BE emission efficiency compared to the DD emission is one of the most significant results of the work reported here.

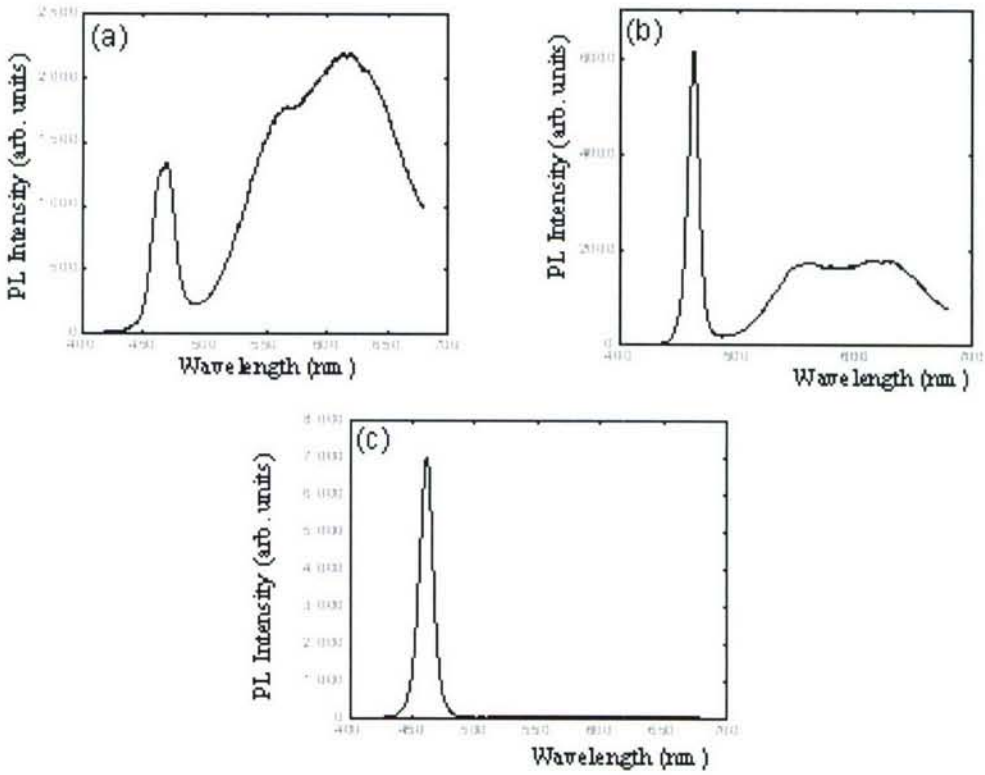

Fig.12. PL spectra of ZnSe nanowires at room temperature: (a) as-grown nanowires; (b) after treatment in a Zn-rich atmosphere at 650 C for 30 minutes, and (c) after treatment in a Zn-rich atmosphere at 650 C for 45 minutes.

3.2 Time-resolved PL measurements

Time resolved measurements using femto-second pump-probe spectroscopy has shed more light on the above results[6]. Transient absorption spectra of stoichiometric and Zn-rich ZnSe nanowires are shown Fig. 13. The observed dynamics shows that state filling effect is the dominant contribution to the transient absorption dynamics when probing with energies below the band gap of ZnSe which is attributed to the occupation of

intrinsic point defects. The relaxation times of these states appears to be of the order of 3-4 ps. Probing with energies above the band gap depicts strong coupling to higher energy states. Carrier dynamics in the Zn-rich grown sample are different from stoichiometric and Se-rich samples. This is mainly attributed to the reduction of point defects and in particular the absence of Zn vacancies located between 1.9 to 2.7 eV. One may conclude that the broad band defect-related photoluminescence in stoichiometric and Se-rich samples is attributed to defect states energetically located between 1.9 to 2.7 eV from the valence band.

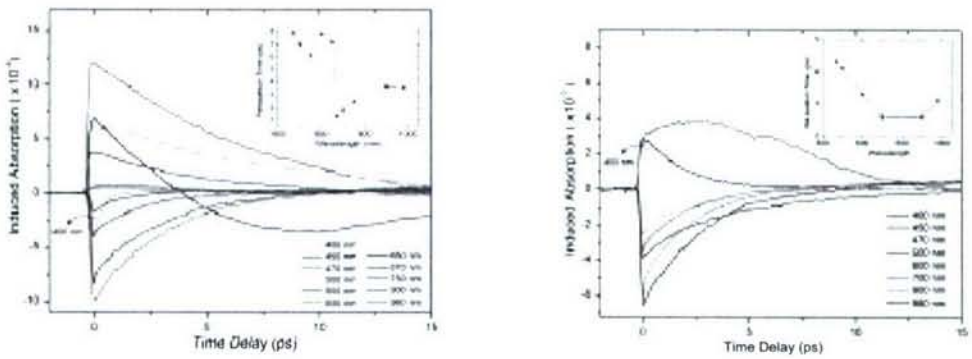

Fig. 13. Time-resolved induced absorption for ZnSe nanowires grown under Se-rich conditions (left) and Zn-rich conditions (right). The sample is excited at 400 nm and probed using white light continuum generation. The various relaxation rates are shown in the inset.

Time-resolved measurements probing the dynamics of optically generated carriers were also carried out on GaAs nanowires using tera-hertz pump-probe spectroscopy. Signal from MBE-grown GaAs nanowires is shown in Fig. 14. We identify the fast 4ps decay in GaAs as the carrier trapping time. The slowing down of the signal decay time as pump power is increased indicates saturation of trap states. As fast trapping of carriers could have a negative impact on the performance of optoelectronic devices such as such as photodetectors and light emitters, processing and growth methodologies developed by us

to eliminate or suppress trap states are of great importance. Photo-conductivity measurements on ZnSe nanowires discussed below indeed show that our optimized growth procedure yields long carrier lifetimes making these structures highly attractive for photodetector applications.

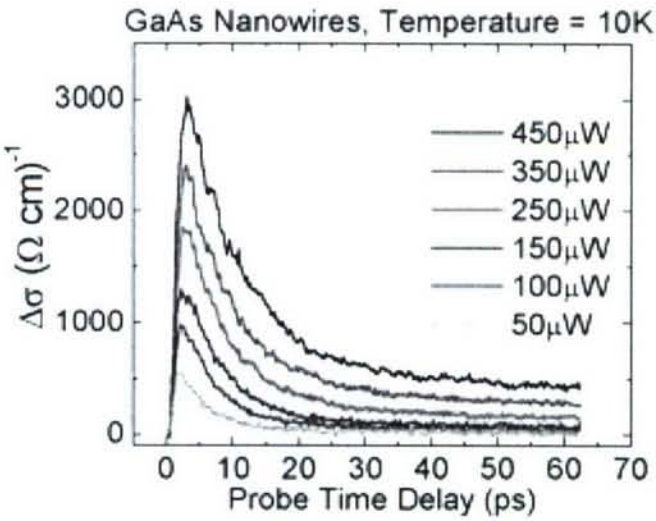

Fig. 14. Tera-hertz differential absorption signal for GaAs nanowires.

3.3 Single nanowire photoconductor

Four-terminal single nanowire photoconductive devices were fabricated using ZnSe nanowires and their electrical and photoconductive properties were studied. Optimization of semiconductor device performance crucially depends on the capability to fabricate ohmic contacts. We were able to achieve good quality ohmic contacts on ZnSe nanwires using Ti/Au multilayers.

ZnSe nanowires were transferred from the as-grown sample to a silicon substrate covered with 100 nm of SiO_2, and their coordinates were recorded using a Raith ELPHY Plus (Raith GmbH) electron beam lithography (EBL) system. A copolymer/PMMA bilayer resist film was deposited on the nanowire-coated substrate, and EBL was used to define

two and four-terminal contact configurations along the length of selected ZnSe nanowires. Typical spacing between contacts was two to four microns. Electron beam evaporation was used to deposit Ti (30 nm) / Au (220 nm) contacts through the resist mask, at a base pressure of ~2 x 10^{-7} Torr. After liftoff and cleaning, samples were annealed in a rapid thermal annealing system at 325 C for 2 minutes, under flowing nitrogen. An SEM image of the fabricated contact structure is shown in Fig. 15.

We observed linear current-voltage characteristics with a typical resistivity of 1 O-cm which is comparable to that of unintentionally-doped n-type ZnSe thin films[7]. The specific conatct resistivity was extracted using a modified transmission line model to be 0.024 comparable to similar contacts in bulk ZnSe samples. This result points to the good quality of the ohmic contacts in spite of the extremely small contact area available in the nanowire geometry.

Detailed photoconductive measurements showed a fundamental absorption edge close to 470 nm (Fig. 16) and no measurable response from the deep levels observed in the PL spectrum described earlier. The measured spectral responsivity showed a peak value of 22A/W at 400nm for a bias of 2.0 V. This is comparable to or better than that of high performance bulk ZnSe photodetectors. The observed high responsivity points to a long excess carrier life time in optimized ZnSe nanowires samples and to the absence of any quenching of carrier lifetime by residual defects.

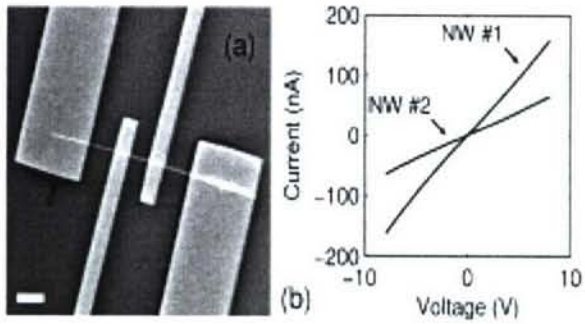

Fig. 15. (a) SEM image of fabricated four-terminal contact structure (scale 4 micron). Bright regions are Ti/Au contacts (b) Two-terminal current-voltage characteristics of representative ZnSe nanowires

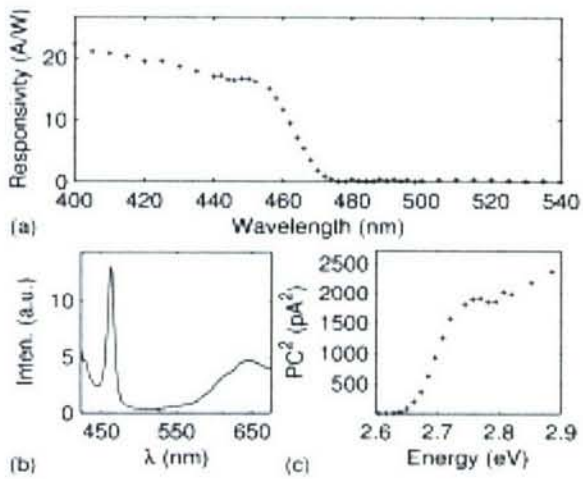

Fig. 16. (a) Spectral responsivity of single ZnSe nanowire with 2V electrical bias applied across Ti/Au electrodes (b) Photoluminescence spectrum of ZnSe nanowire array (c) Normalized and squared photocurrent spectrum

3.4 Room temperature Ferromagnetism in ZnO:Mn nanowires

Above room-temperature ferromagnetism was achieved in Manganese (Mn) doped ZnO nanowires[8]. Structural characterizations by TEM and EDXS showed that Mn was uniformly incorporated into the ZnO lattice forming single-phase, single crystalline nanowires. Mn concentration was determined using EDXS and Ion Coupled Plasma Mass Spectrometry (ICPMS) [Perkin Elmer Sciex ELAN DRC II]. ICPMS results showed 1 to 4% of Mn in all samples studied.

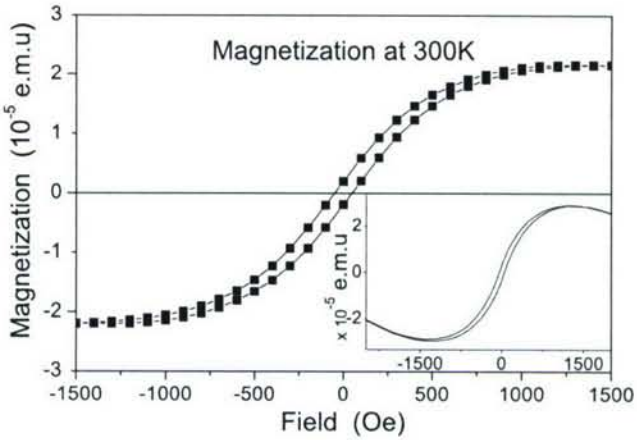

Fig. 17. Hysteresis loop (M-H curve) of Mn-doped ZnO nanowires with ~1 atomic % Mn at 300 K. The inset shows the as-obtained SQUID data, including the diamagnetic contribution from the Si substrate.

Magnetic properties of the nanowires were studied using a superconducting quantum interference device (SQUID) magnetometer [Quantum Design MPMS XL-7S]. SQUID measurements showed a distinct hysteretic magnetization loop superimposed on a linear diamagnetic contribution from the silicon substrate, as shown in Fig. 17. All the Mn-doped nanowires samples studied showed ferromagnetic behaviour well above room temperature. Fig. 18 shows the variation of magnetization, M with temperature, T, measured in an applied field of 100 Oe upon warming the sample which had been cooled from 300 K to 1.8 K in an applied magnetic field of 100 Oe. The magnetization decays very slowly with increasing T over the range studied. The Curie temperature T_c is well above room temperature, but it is hard to determine the exact value, since the value of T_c is rather high, exceeding the range of our measurements, i.e., $T_c > 400$ K. From the observed saturation magnetization $M_s \sim 2.0\text{-}3.0 \times 10^{-5}$ e.m.u, the magnetic moment per Mn atom is estimated to be in the range from 0.30 μ_B to 1.2 μ_B, somewhat less than the maximum spin moment of 5 μ_B per Mn^{2+}.

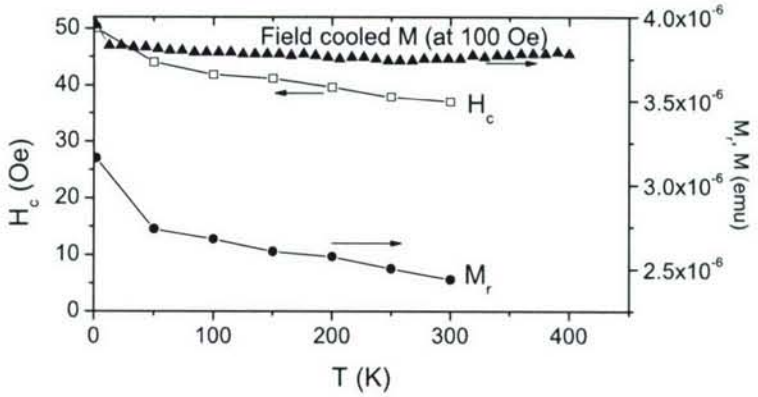

Fig. 18. Temperature dependence of remnant magnetization (M_r), coercive field (H_c) and field cooled magnetization (M-T at 100 Oe).

Theoretically, ferromagnetism in DMS can be understood in terms of carrier-mediated exchange coupling between the localized spins of the transition metal ions[9]. However, unlike Mn-doped GaAs or other III-V materials, in II-VI materials such as ZnO, Mn behaves as an isovalent impurity providing no additional carriers. Thus there is great interest in understanding the origin and nature of free carriers in ZnO:Mn. To this end, we fabricated single nanowire back-gated field effect transistor structures using Mn-doped ZnO nanowires by an approach similar to that described earlier for ZnSe nanowires. Through detailed current-voltage measurements[10] we established that transport is dominated by electrons, i.e., the nanowires are n-type. The temperature dependence of carrier concentration and mobility extracted from the measurements is shown in Fig. 19. From the results it is clear that free carries in Mn-doped ZnO nanowires are degenerate. The mobility is seen to be dominated by impurity scattering which we attribute to intrinsic defects.

Fig. 19. Temperature dependence of carrier concentration (diamonds) and degree of degeneracy (circles), and (b) Measured temperature dependence of field effect mobility (circles) plotted with asymptotically degenerate (dash-dot) and nondegenerate (dashed) temperature dependences

4 Theory and Modeling

4.1 Design of nanowire array based photonic cavities

With an aim to developing designs for high-performance structures of finite nanowire arrays we performed extensive modeling of electromagnetic response of nanowire arrays using the Finite-Difference Time Domain (FDTD) approach. Although the photonic band structure of infinite arrays of nanowire-like objects has been well studied in the past, practically important finite size arrays of a few 10 nanowires across have been largely overlooked. Based on our calculations we identified some surprising facts[11,12]

i. The quality factor of finite arrays depends very strongly on the array boundaries in relation to the lattice vectors of the array.

ii. Relatively large Q-factors could be achieved in moderately sized arrays that are only about 10 nanowires across.

iii. In nanowires standing vertically on a substrate, the leakage of high-Q modes along the axial direction is significant only at the substrate end and this could be suppressed having a small length of a low refractive index material at the foot of the nanowires.

As an example, Fig. 20 shows the fundamental mode in a 13x13 square nanowire array with geometry such that the sides are of the array are along the symmetry axes of the unit cell. This geometry optimizes the Q-factor.

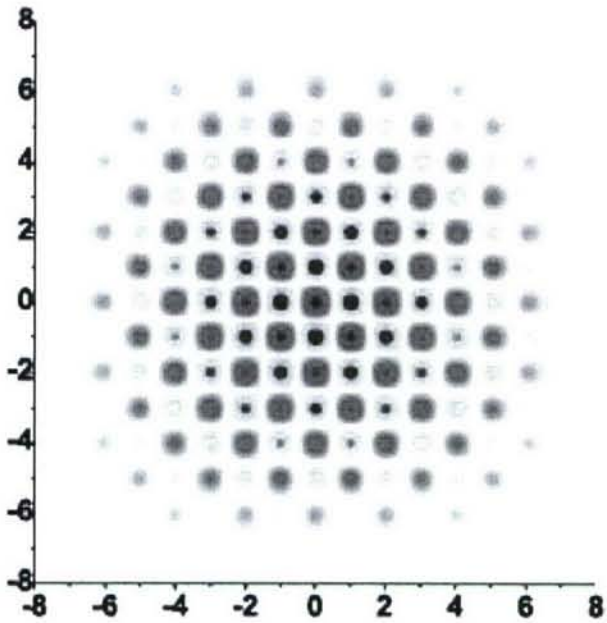

Fig. 20: The fundamental mode in a finite square array of nanowires (size 13x13) with sides along the symmetry axes of the array. This mode has a high Q of 150,000 and a normalized mode volume of only 8. The Q factor reduces by two orders of magnitude when the sides of the square are oriented at 45 degrees to the symmetry axes.

The above result was obtained using a 2-D simulation which implicitly assumes the nanowires to be infinitely long. We performed full 3-D simulations to estimate the leakage of high-Q modes along the axial direction and identified a scheme for effectively suppressing the leakage using a gloved geometry as illustrated in Fig. 21.

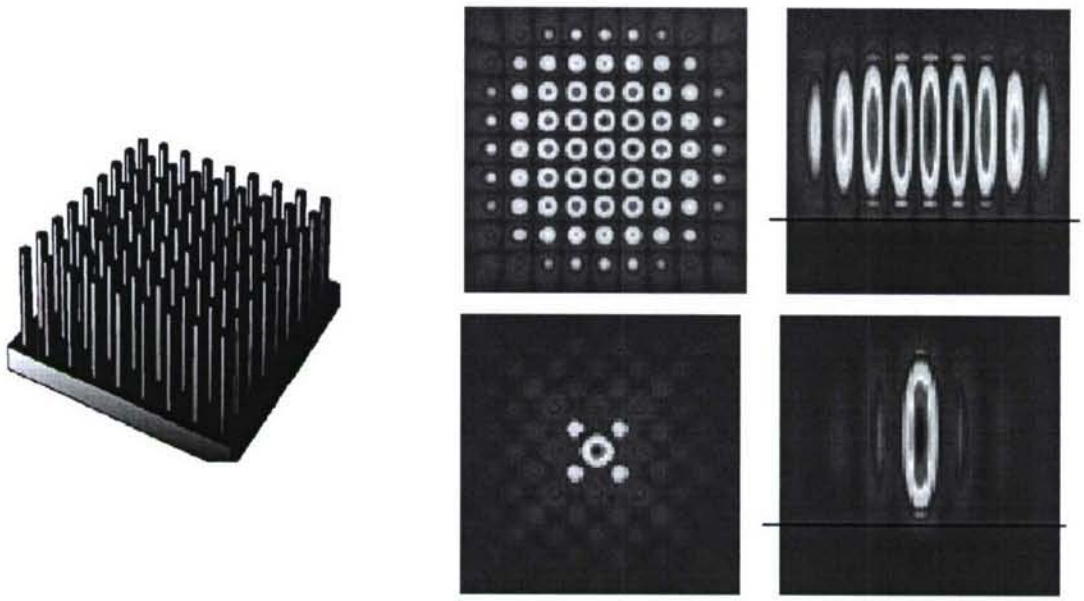

Fig 21. Confined modes realized using array geometry shown on left. The top two panels show the a confined mode in a 9x9 array while the bottom panels show a defect mode in a 7x7 array with a defect at the centre. Left and right panels show vertical and horizontal cross-sectional views. In both cases the leakage into the subsrate is suppressed using a gloved geometry which has a small section of a lower refractive index material grown at the root of the nanowires.

4.2 Theory of Excitons in nanowires

Although some authors have reported calculations of exciton states in nanowires in the past several essential features of electron-hole dynamics have been overlooked in all published calculations. We developed a theory of quantum confined exciton in nanowires including important effects of heavy-hole light-hole coupling and dielectric confinement effects[13]. Because of strong quantum confinement the electron-hole interaction along the transverse dimension of the nanowire can be often treated perturbatively but strong electron-hole correlations along the axial dimension calls for a non-perturbative treatment. Our approach to this problem involves deriving an effective one-dimensional

potential for the Coulomb interaction and then solving the resulting effective one-dimensional equation numerically. As single sub-band approximations commonly employed in quantum wire calculations is reasonable only when the wire radius is very small, we developed a multi-sub-band scheme in which the radial eigen functions of the electron and hole are expanded into a number of near-band edge states. This results in a system of coupled 1-D Schrodinger's equations that are solved together. Another novel feature of our approach is the way radial-axial separation is handled. As heavy-hole light-hole mixing renders the hole eigen functions dependent on the axial momentum, the radial and axial motions do not strictly separate in nanowire exciton dynamics. We solved this problem by using the zero axial momentum hole eigen functions as the basis states. This leads to k-dependent coupling between the effective 1-D inter sub-band dynamics even in the absence of Coulomb interaction but causes no further complications.

Although our sub-band dependent effective 1-D potentials depends on specific material parameters including effective masses and dielectric constants of the nanowire and its surrounding, the potential could be fitted rather accurately to the form $V(z) = A/|z+z_0|$, where A and z0 are material and geometry dependent constants. Such simplified forms, although not used in our calculations, are extremely useful in calculating various Coulomb interaction dependent effects in nanowires such as donor and accepted states, DA pair energies, final state energies involved in photo-emission measurements etc.

Fig. 22 shows calculated exciton binding energies in GaAs and ZnSe nanowires. The binding energies are strongly dependent on the dielectric mismatch between the nanowire and the surrounding matrix. Combined effects of quantum and dielectric confinement lead to a large enhancement of the exciton binding energy. In 20nm diameter GaAs nanowires in air, for example, the exciton binding energy is enhanced by a factor of ~25

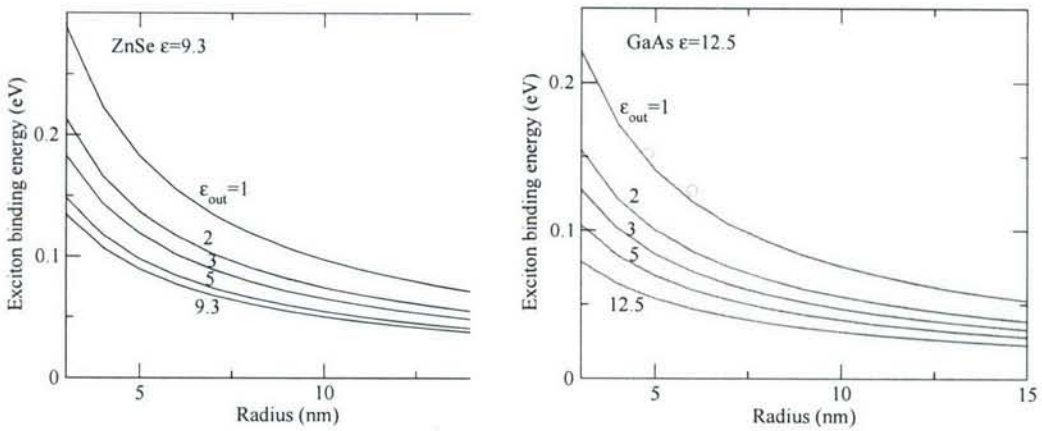

Fig. 22 Calculated exciton binding energies in ZnSe (left) and GaAs (right) nanowires as a function of the nanowire radius for various values of the dielectric constant of the surrounding medium (e_{out}).

Our calculations also show that the light-hole heavy-hole mixing in the lowest energy exciton is so as to create a strong anisotropy in the oscillator strength for inter-band transitions with oscillator strength for light polarization along the axis of the nanowire larger than that for perpendicular polarization. We predict a degree of polarization of 60% in ZnSe nanowires. This should be augmented by the polarization selectivity due to dielectric mismatch arising from pure electrostatic considerations. Overall, free standing ZnSe nanowires are expected to show a very strong degree of polarization of 98%.

4.3 Second harmonic generation from nanowires

Centro-symmetric materials such as silicon has a vanishing second-order dipolar susceptibility ($\chi^{(2)}$), while in zinc-blende materials only components of the type $\chi_{xyz}^{(2)}$ are non-zero. In both cases, second harmonic generation from such materials is either very weak or occurs only in certain special geometries as contributions from higher order

quadrupolar terms is generally small. However, nanostructures of even centro-symmetric materials could exhibit strong quadrupolar response because of large electric field gradients at the surface. We developed a theory of second harmonic generation from centro-symmetric nanowires due to such surface contributions[14]. Our results predict a strong polarization anisotropy of second-harmonic signal and the response is strongest when the incident light is polarized parallel to the axis of the nanowire.

5 Work in progress

Owing to the small band gap and long carrier lifetime, InSb is a favored material for infra-red (IR) detector applications. Development of InSb nanowires is of great interest for next generation high-performance IR detector arrays. We have done preliminary VLS growth studies on InSb nanowires on silicon substrate. The composition and crystalline quality of the wires is seen to be very sensitive to growth conditions. We obtained stoichiometric nanowires is a narrow temperature range of 420 to 450 C. transport measurements showed that stoichiometric InSb nanowires are n-type with a large carrier density of ~ $5x10^{18}/cm^3$ and mobility in excess of several thousands of cm^2/Vs. These initial results hold great promise for device applications and warrant further study.

6 Conclusions

We developed optimized fabrication methodology for several II-VI and III-VI nanowires by VLS based growth mechanism. By controlling growth conditions and by post-growth treatment methods highly crystalline and relatively defect free nanowires were obtained. Growth optimization was assisted by detailed optical and transport measurements that helped reveal the origin and nature of defects and frere carrier dynamics in nanowires. Most significant accomplishments of the current effort are

i. Identification of Zn-vacancy related defects as responsible for mid-gap emission and development of annealing methodology to obtain efficient band-edge luminescence in ZnSe nanowires

ii. Realization of single nanowire ZnSe photodetector with an exceptionally high responsivity of 22A/W

iii. Growth of Mn-doped ZnO nanowires and discovery of above room-temperature ferromagnetism in these nanowires.

iv. Growth of highly ordered nanowire arrays using alumina template masks

v. Growth of high quality InSb nanowires with high carrier mobility

vi. Modelling and design of finite nanowire array based high-Q photonic cavities

vii. Development of a realistic theoretical model for excitons in nanowires

These results have revealed a rich potential in nanowires for optical applications. Topics that are particularly important and interesting for further study are, InSb nanowires for IR detection and perfecting of ordered nanowire array growth required to realize photonic cavity designs presented by us.

7 References

1. Z.H. Wu, X.Y. Mei, D. Kim, M. Blumin and H. E. Ruda, Appl. Phys. Lett., **81**, 5177 (2002); N138; N149

2. Usha Philipose, "Growth and characterization of semiconductor nanowires", Ph.D. thesis submitted to University of Toronto (2006).

3. Z. H. Wu, J. Gierak, E. Bourhis, A.-L. Biance, and H. E. Ruda, Proc. SPIE Int. Soc. Opt. Eng. **5971**, 597117 (2005).

4. X. T. Zhang, Z. Liu, K. M. Ip, Y. P. Leung, Q. Li, S. K.Hark, J. Appl. Phys. **95**, 5752 (2004).
5. U. Philipose, S. Yang, T. Xu, and Harry E. Ruda, Appl. Phys. Lett. **90**, 063103 (2007)
6. A. Othonos, E. Lioudakis, U. Philipose and H. E. Ruda, "Unltrafast carrier dynamics in bandedge and deep defect ZnSe nanowires" (Submitted to Appl. Phys. Lett.)
7. J. Salfi, U. Philipose, C. F. de Sousa, S. Aouba, and H. E. Ruda, Appl. Phys. Lett. **89**, 261112 (2006).
8. U. Philipose, S. V. Nair, S. Trudel, C. F. de Souza, S. Aouba, R. H. Hill, and H. E. Ruda, Appl. Phys. Lett. **88**, 263101 (2006).
9. T. Dietl, H. Ohno, F. Matsukura, J. Cibert and D. Ferrand, Science **287**, 1019 (2000); S. J. Pearton, C. R. Abermathy, M. E. Overberg, G. T. Thaler, D. P. Norton, N. Theodoropoulou, A. F. Habard, Y. D. Park, F. Ren, J. Kim and L.A. Boatner, J. Appl. Phys. **93**, 1 (2003).
10. J. Salfi, U. Philipose, S. Aouba, S. V. Nair, and H. E. Ruda, Appl. Phys. Lett. **90**, 032104 (2007).
11. T, Xu, S. Yang, S. V. Nair, and H. E. Ruda, Phys. Rev. B **72**, 045126 (2005).
12. T. Xu, S. Yang, S.V. Nair, and H. E. Ruda, Phys. Rev. B **75**, 125104 (2007).
13. S. V. Nair and H. E. Ruda, "Theory of excitons in nanowires" (in preparation).
14. H. E. Ruda and A. Shik, J. Appl. Phys. **101**, 034312 (2007).